18TH WORLD CONFERENCE ON EARTHQUAKE ENGINEERING
WCEE2024
MILAN

MILAN, ITALY
30TH JUNE - 5TH JULY 2024

www.wcee2024.it

THE NEW SELF-ANCHORED SUSPENSION (SAS) SAN FRANCISCO BAY BRIDGE - ITS RESPONSE TO A SMALL EARTHQUAKE

M. Çelebi[1]

[1] U.S. Geological Survey Earthquake Science Center, Moffett Field, Calif., USA, celebi@usgs.gov

Abstract: *This paper presents a summary of previously published work (Celebi 2023) related to the. new Self-Anchored Suspension (SAS) bridge that went into service within the last decade as a replacement for the older truss bridge spanning between Yerba Buena Island and Oakland, California, within the San Francisco Bay Area. During the October 19, 1989 M6.9 Loma Prieta earthquake, which occurred ~100 km south of the Bay Bridge, a section of the upper deck of the truss bridge fell onto the lower deck – thus closing this important lifeline between San Francisco and Oakland. The SAS is unique, self-anchored, and suspended by a single tower that is pivotal in trafficking the cable and hanger system to support the decks. The SAS bridge is extensively instrumented by the California Geological Survey's Strong Motion Instrumentation Program (CSMIP). There are approximately 85 channels of accelerometers in the seismic monitoring system that recorded the October 14, 2019 Mw4.6 Pleasant Hill earthquake. The data allow a complex but identifiable coupled response of the deck, tower, and cable system. Both acceleration and displacement time-history data are used to extract significant frequencies using system identification methods, including spectral analyses. Results are compared to those from finite-element-model (FEM) analyses carried out during the design and analysis process of the bridge in 2002 (Nader et al. 2002). There are differences between FEM analyses results and those from the low amplitude shaking caused by a seismic event. An apparent frequency (period) of the SAS bridge is assessed (approximately 5.2 seconds). In a plot of deck length versus period, there is an almost linear relationship with periods of other regular suspension bridges, such as the Golden Gate Bridge and the Carquinez Bridge, both in the San Francisco Bay.*

1. Introduction

This paper presents a slightly revised and shortened summary of previously published work (Celebi 2023).

At ~100 km from its epicenter **of** the October 17, 1989, M_w6.9 Loma Prieta, California earthquake (LPE), a segment of the upper deck of the old truss bridge component of the San Francisco-Oakland Bay Bridge (SFOBB) system fell onto its lower deck. Figure 1a (Penzien et al., 2003) displays this signature structural failure of that event which resulted in closure of the most important lifeline within the San Francisco Bay Area (SFBA), the SFOBB system, which serves as the main transportation connection between the San Francisco Peninsula and the eastern Bay Area. The damaged bridge was rapidly repaired but was determined that the old truss bridge of SFOBA system was seismically vulnerable (Penzien et al., 2003). **I**n 2013, the Self Anchored Suspension [SAS] Bridge) was opened to service. Figure 1b shows a picture of both the SAS and the old truss bridge before the old truss bridge was razed. The map in Figure 1c displays the SFBA communities, locations of the six long-span bridges (including the SFOBB), and approximate locations the San Andreas and Hayward Faults. These two faults are the major geological sources of seismic hazards for the built environment in the SFBA. The whole SFOBB system is equipped with seismic monitoring system by the California Strong Motion Instrumentation Program (CSMIP) of the California Geological Survey (CGS). The SAS seismic monitoring array (accelerometers, tiltmeters, and displacement sensors) has been assigned he station number 58600.Wheras there are several recorded responses of the SAS from small earthquakes, data recorded during

a small event (the October 14, 2019, M_w4.6 Pleasant Hill earthquake, [22:33:42.810 PDT, coordinates 37.9380° N, 122.0570° W, and 14.0 km depth]) that occurred at an epicentral distance of 29.9 km from the SAS (www.strongmotioncenter.org, last accessed August 11, 2023) are used in this paper. The epicentral location of this event relative to the SAS and the SFBA is illustrated in Figure 1c. Hence, the purpose of this paper is to study the response and behavior of the SAS Bridge during the referenced event only. The scope of this paper comprises analyses of real-life behavior of the bridge using recorded data but does not include FEM analyses. In-depth details of the Loma Prieta earthquake and its effects are in the USGS publication: https://www.usgs.gov/programs/earthquake-hazards/science/loma-prieta-earthquake-professional-papers).
Design details of the SAS are discussed by others [Sun, Manzanarez, and Nader (2004); Frick (2016); McDaniel, Uang, and Seible (2003); Nader, Duxbury, and Maroney (2014); and Nader, Lopez-Jara, and Mibelli (2002)]. Nader, Lopez-Jara, and Mibelli (2002) and Nader, Duxbury, and Maroney (2014) describe seismic hazard evaluations of SAS. In summary, a safety-evaluation earthquake (SEE) and a functional evaluation earthquake (FEE) have been defined. The SEE was defined by a probabilistic seismic hazard analysis with a 1500-year return period. Design for FEE requires that the SAS provide immediate full service with essentially elastic performance. The SEE design requires the bridge to be functional with or without repairable damage that can be repaired within a few days (Nader, Lopez-Jara and Mibelli [2002] and Nader, Duxbury, and Maroney [2014]). Zero-period accelerations (ZPA) for the design events have not been revealed. They state that (a) the design of the SAS is governed by the safety evaluation earthquake (SEE), and (b) the analyses using this criterion computed the longitudinal, transverse, and vertical fundamental periods (frequencies) of the SAS as 3.80s (0.263 Hz), 3.64s (2.75 Hz), and 4.50s (0.222Hz).

It is important to re-state that, in this paper, recorded data from sensors deployed at components of the SAS are used. Therefore, the fundamental periods (frequencies) reported by Nader, Lopez-Jara, and Mibelli (2002) in the global longitudinal, transverse, and vertical coordinates of the bridge are not directly comparable with those dynamic response characteristics to be identified using the data from the small 2019 earthquake.

2. The SAS structure and foundation

Modified from www.strongmotioncenter,org (last accessed August 31, 2023), Figure 2 shows schematics of the vertical and plan views of the overall SAS structural system. The SAS is the bridge structure between Pier W2 and Pier E2 (including the tower and foundations), as seen in Figure 2a. Its main deck comprises dual orthotropic steel box girders, each having a width of 27.88 m (91.47 ft). The box girders are not attached to the tower. The westbound (W) and eastbound (E) girders are connected by steel crossbeams and are suspended with hangers from cables, which, in turn, are hung over a saddle system, and thus, supported at the top of a single steel tower at an elevation of 160 m (524.93 ft). The “Self-Anchored Suspension” means that the cables that are anchored at Pier E2 and looped around Pier W2 through a saddle at top of the tower. Unlike the traditional two-tower suspension bridges, SAS has no anchorages as is with the two suspension SCOBB system bridges between San Francisco and Yerba Buena Island, west of the SAS, or the Golden Gate Bridge between San Francisco and the Marin Peninsula. In Figure 2a, I added in-plan orientations as longitudinal (L) along the length of the deck, and transverse (T) perpendicular to the length of the deck as the global coordinates of the overall SAS structure. The total length of the deck of the bridge is 622.5 m (2042 ft).

The unique design of the tower depicted in Figure 2b comprises four steel shafts interconnected by steel shear links designed for inelastic behavior. The shafts are rigidly connected at the saddle at the top of the tower. The shear links have been cyclic tested (McDaniel, Uang, and Seible [2003]). Piers W2 and E2, each comprise a concrete cap beam that is supported by concrete columns. The columns of Pier W2 are tied down to the foundation.

The foundation of the bridge comprises: (a) At Pier W2, a concrete footing on top of 2.5 m cast-in-drilled-hole (CIDH) concrete piles at the westbound side. (b) At the tower, a concrete footing on top of a total of thirteen 70-meter-long piles (2.5-meter-diameter concrete piles with steel casing and 2.2-m-diameter CIDH piles, all rock socketed at an elevation of -59.5m). (c) At Pier E2, each footing cap (below the westbound [W] and eastbound [E] decks) rests on eight 105.5-meter-long, 2.5-meter-diameter cast-in-steel-shell (CISS) piles. (d) The W and E footing caps are connected by a 5.7-meter-deep concrete beam. (e) All piles are socketed to rock. An “approximate rock line” and an “approximate grade” are shown in Figure 2b. The rock is described as sedimentary, and is overlain by alluvium (www.strongmotioncenter.org, last accessed August 11, 2023). Nader, Duxbury, and Maroney (2014) describe the rock as Franciscan Formation and the alluvium as consisting of sandy clays and sand of the Alameda Formation.

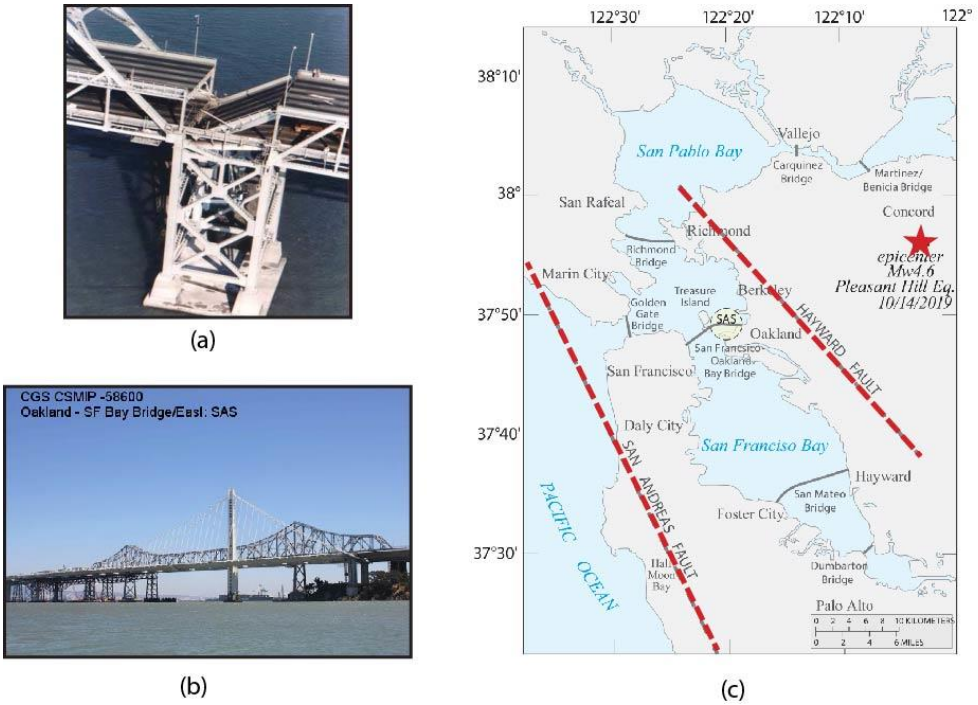

Figure 1. (a) Signature photo of the fallen upper deck section of the old Bay Bridge between Yerba Buena Island and East Bay (adopted from Penzien et al., 2003). (b) Photo of the old truss bridge and the new SAS Bridge (white colored); from www.strongmotioncenter.org, last visited accessed August 11,2023). (c) Map of the San Francisco Bay Area depicting the locations of six major long-span bridges, including the SFOBB and SAS (map is modified from Nader, Lopez-Jara, and Mibelli, 2002).

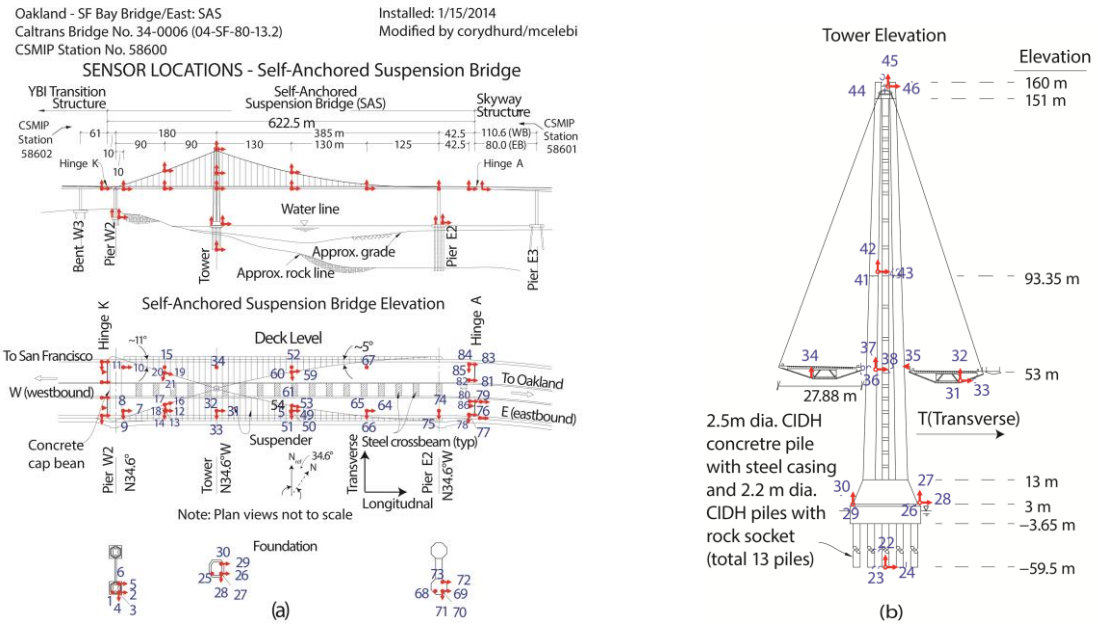

Figure 2. (a) Schematic showing vertical and plan views and some details of the foundation. The red arrows and dots refer to the location and orientation of the particular channel of accelerometer. (b) Vertical elevation of the tower and decks at the tower location. Figure modified from www.strongmotioncenter.org. CIDH pile refers to cast-in-drilled-hole pile.

3. Seismic instrumentation array and recorded earthquake data

Figure 2 also shows some of the locations and orientations of most of the seismic monitoring sensors (accelerometers, tiltmeters, and displacement sensors), the north (N) and reference north (Nref), as well as the global coordinates (longitudinal [L] and transverse [T]). I assigned the horizontal cable-specific longitudinal and translational orientations (C1L and C1T, respectively) for the side span and (C2L and C2T, respectively) for the main span. CSMIP reports the largest peak acceleration was 0.13g (channel 76 at hinge A of the eastbound deck), with a processed max peak of 127.79 cm/s^2 (www.strongmotioncenter.org, last accessed August 30, 2023). The largest displacement is recorded as 0.95 cm (vertical at the westbound cable). It is important to note herein that the recorded response data presented by CSMIP via www.strongmotioncenter.org are both (i) raw (unprocessed accelerations) and (ii) processed "avd" (acceleration [a], velocity [v], and displacement [d]) versions. Processing was completed by CSMIP. Details of processing filters are always included in the headers of each "avd" data set for each channel. In this study, only processed "avd" data sets are used.

4. Analyses of recorded data

4.1. Time Histories at Tops of Foundation Footing, Tower, and Downhole:

Considered as the horizontal and vertical input excitation of the SAS structural system that are supported by the tops of foundation footings, time-histories of equiscaled accelerations and displacements are depicted in Figure 3 for Piers W2, E2 and the tower. As expected, the amplitudes of accelerations (longitudinal, transverse, and vertical) are greater for those footing with top locations that are in deeper alluvium (Pier E2 and the tower location), as compared to those at Pier W2, which is on rock (channels 4, 5, and 6). Simply stated, and as expected, motions at the alluvial locations are amplified relative to those at rock locations.

The strong shaking duration of input horizontal motions are computed for accelerations (recorded by channels 23 and 24 at the bottom of borehole (rock at elevation -59.5m) as shown in Figures 4a and 4b using the summed squared horizontal accelerations method (Trifunac, M. D. and Brady, 1975; Boore and Thompson, 2014). Herein, the 5-95% method defines the strong-shaking duration as 13.25 s as an estimate of the duration of strong shaking input motions to the SAS. Later in this paper, I refer to this figure in discussions of the elongated duration of shaking at the superstructure of the SAS.

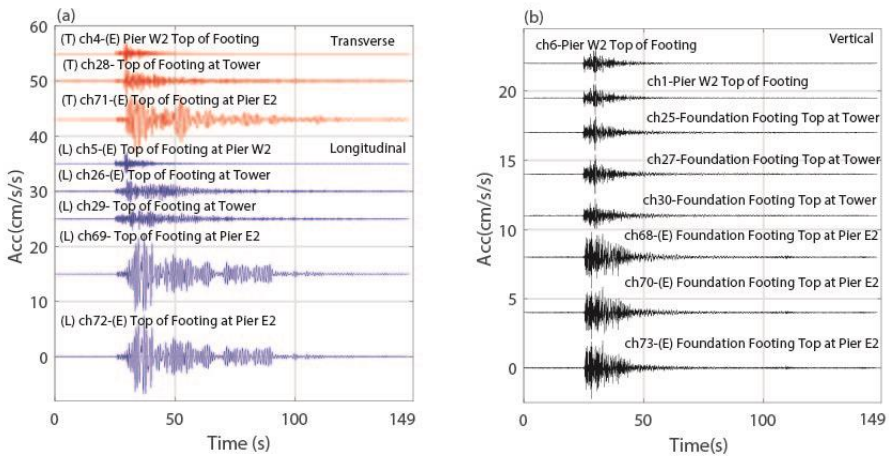

Figure 3. (a) Translational and (b) longitudinal time-history plots of accelerations at the top of foundation footings of Piers W2 and E2, and the tower.

4.2. Acceleration and Displacement Time Histories at SAS Superstructure (Deck, Tower, and Cables) and Foundation Tops

Acceleration and displacement time histories of the tower, deck, cables, and foundation tops are plotted in equiscaled frames for the longitudinal direction in Figure 5, the transverse direction in Figure 6, and the vertical direction in Figure 7. For all structural time histories, the figures show the strong-shaking duration that is longer than the input motion strong-shaking duration, as discussed earlier and displayed in Figure 4a. Particularly in the displacement time histories of numerous channels (Figures 5, 6, and 7), there is strong evidence of a repetitious beating effect that will be discussed in detail later in this paper.

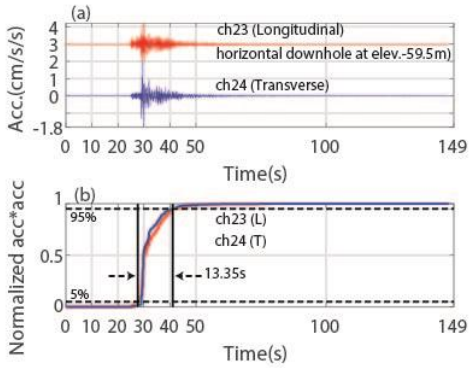

Figure 4. (a) Accelerations at horizontal downhole at elevation -59.5m (at rock) and (b) estimated ground motion duration. T~13.35s.

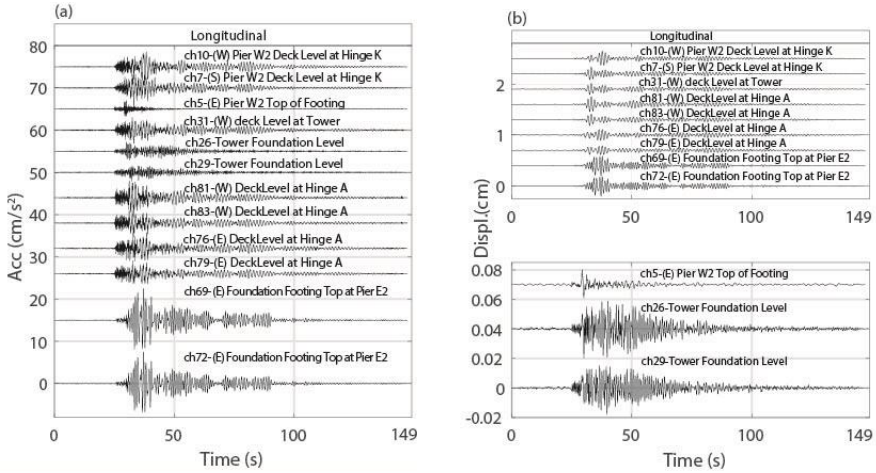

Figure 5. In the longitudinal direction, (a) plots of equiscaled time histories of accelerations and (b) displacements with different vertical scales in ttwo frames.

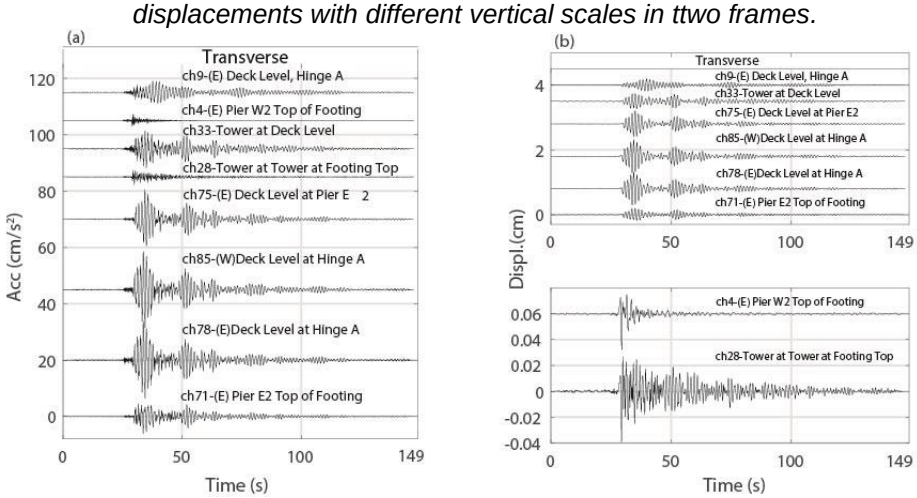

Figure 6. In the transverse direction, (a) plots of equiscaled time histories of accelerations and (b) displacements with different vertical scales in ttwo frames.

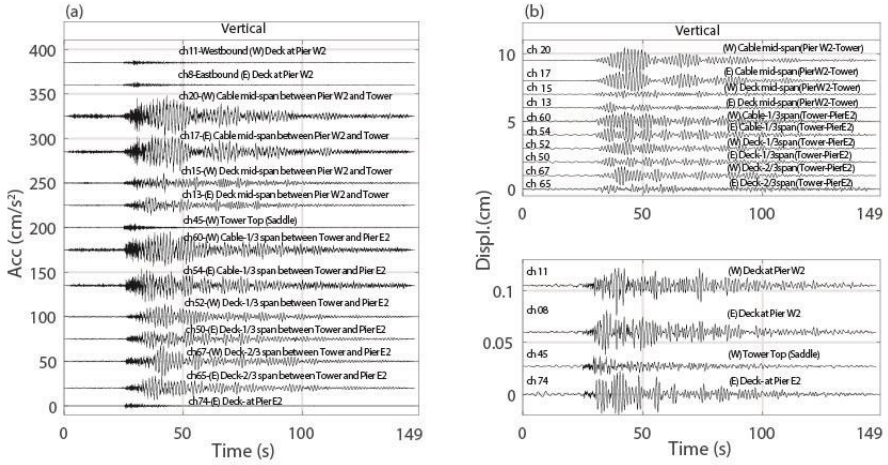

Figure 7. In the vertical direction, (a) plots of equiscaled time histories of accelerations and (b) displacements with different vertical scales in ttwo frames.

4.3. Identification of structural dynamic characteristics

As stated earlier, sensors are deployed at the deck, tower, cables, and the foundation of the SAS. This means that the frequencies identified from the data set are those of the structural components, respectively and not the global coordinates of the SAS.

Amplitude spectra of longitudinal, transverse, and vertical displacements (double integrated from acceleration recorded by the channels of accelerometers) are computed. This is followed by computation of spectral ratios. Displacements are used to better represent the low frequencies (<0.5Hz). Longitudinal spectral ratios are computed with respect to (w.r.t) ch23 (the longitudinal downhole channel at elevation -59.5m at rock). Similarly, transverse spectral ratios are computed w.r.t ch24 (the transverse downhole channel) and vertical spectral ratios are computed w.r.t ch22 (the vertical downhole channel). In Figure 8a (left), both the amplitude spectra of longitudinal displacements and the spectral ratios (w.r.t. the amplitude spectrum of downhole ch23) allow identification by peak picking of the lowest frequency at ~0.30 Hz and others at 0.71, 0.83, and 2.08 Hz. This first modal frequency at ~0.30 Hz is clear only in these plots of spectral ratios of amplitude spectra of displacements and not in those computed from accelerations. The frequency at 0.71 Hz likely appears due to coupling with modes other than longitudinal. Both the amplitude spectra and spectral ratios are repeatable for all channels in each frame. In Figure 8a (center), spectral ratios computed using amplitude spectra of transverse displacements allow identification of frequencies at ~0.33, 0.77, 1.78, and 3.13 Hz. Again, both the amplitude spectra and spectral ratios are repeatable for all channels in each frame. Similarly, in Figure 8a (right), spectral ratios computed using amplitude spectra of vertical displacements of deck and cable locations allow identification of frequencies at ~0.25 and ~0.68-0.90 Hz.

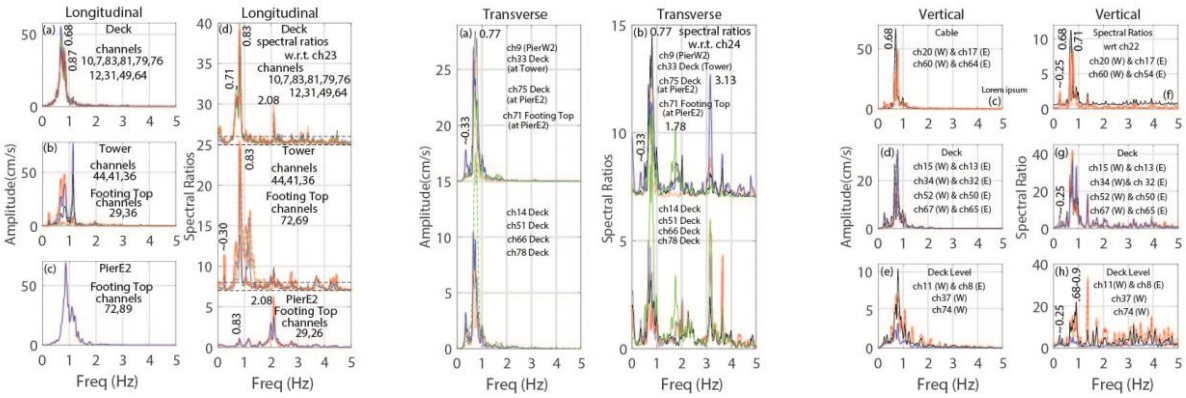

Figure 8. (Left) Longitudinal amplitude spectra of displacements and spectral ratios. Frequencies are identified from the corresponding spectral ratios computed using amplitude spectra. Similarly using, (center) transverse displacements and (right) vertical displacements. Transverse frequencies are identified as ~0.33, 0.77, 1.78, and 3.13 Hz and vertical frequencies are identified as ~0.25 and ~0.68-0.90Hz. In each frame, the figures show repeatability of the peaks according to the channels in descending order.

4.4. System identification and first modal shapes, frequencies and damping

Modal shapes, frequencies (f), and critical damping percentages (ξ) are identified using Subspace State Space System Identification (N4SID), coded in Matlab (Mathworks, 2020). N4SID background is provided in Van Overschee and De Moor (1994, 1996) and Ljung (1999). N4SID is applied using several orientations and structural-component-specific displacement data to estimate the modal shapes, f and ξ. The extracted translational and vertical first-modal shapes for the deck are provided in Figure 9a. The identified transverse first-mode frequency (period), $f_1(T_1)$, is 0.36 Hz (2.79 s), and the critical damping percentage is 2.11%. The identified vertical first-mode frequency (period), $f_1(T_1)$, is 0.24 Hz (4.14 s), and the critical damping percentage is 2.64%. It is noted that the deck first-mode shapes in the vertical direction for the side span and main span are in the opposite sense vertically. This is because there is no physical restraint of the deck at the tower location and the hanger-cable-tower pull action for the main-span forces the side-span to displace in the opposite sense vertically. Similarly, in Figure 9b, the extracted first longitudinal and transverse mode shapes for only the tower are shown. The identified longitudinal first-mode frequency (period), $f_1(T_1)$, is 0.47 Hz (2.14 s) and the critical damping percentage is 3.14% (all provided in the figure). The identified transverse first-mode frequency (period), $f_1(T_1)$, is 0.36Hz (2.79 s), and the critical damping percentage is 4.83%, both of which are inserted in the figure.

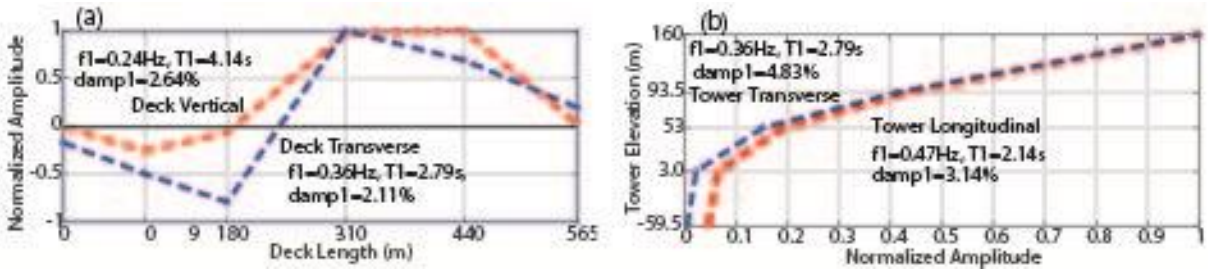

Figure 9. First-modal shapes , frequencies, and critical-damping percentages of the deck in the transverse and vertical directions and (b) of the tower in the longitudinal and transverse directions.

The first-modal frequencies identified by the N4SID method compare well with those identified from the spectral ratios. However, the identified critical damping percentages does not compare well with that assessed by logarithmic decrement method introduced later in the paper. All identified frequencies and critical damping percentages are summarized in Table 2 later in the paper.

4.5. Beating effect

Beating effects have been observed in response data of many buildings and have been studied in-depth by Boroschek and Mahin (1991), resulting in a formula for computing beating periods of buildings when torsional and translational natural periods of vibration are close (or closely coupled):

$$T_b = 2/|f_1-f_2| = 2T_1T_2/|T_1-T_2| \quad (1)$$

where T_1 and T_2 are the translational and torsional periods, respectively. By definition, the beating period (T_b) is twice the inverse of beating frequency (f_b). ($T_b = 2/f_b = 2/|f_1-f_2|$). The beating effect is mainly observed when the damping in the structural system is small and occurs when repetitively stored potential energy, produced during coupled translational and torsional deformations, turns into repetitive vibrational energy (Çelebi, 2018). There are only a few publications that refer to beating effects of long-span bridges using earthquake response data (e.g. that of the Carquinez [California] Suspension Bridge array during the M_w 6.0 South Napa earthquake of August 24, 2014 [Çelebi et al., 2019]). However, in studies of three sets of earthquake response data acquired from Golden Gate Bridge, beating effect was not observed (Çelebi, 2012). Furthermore, there are a limited number of studies (including the study by Boroschek and Mahin (1991)) related to tall buildings that assessed the beating phenomena from recorded earthquake response data. A recent study of the 61-story Salesforce Tower (San Francisco's tallest building) during the January 4, 2018 M_w 4.4 Berkeley earthquake (Çelebi et al., 2019) also assessed a beating effect. Separately, in a recent study, an approach to quantify the effect of beating in lengthening the vibrational duration, and therefore, the vibrational energy impacting f tall buildings is presented in (Çelebi, 2018).

For this study, beating effect on SAS is displayed in Figures 10a, b, and c. Several cycles of beating extends the duration of strong shaking in the translational (ch51) and vertical accelerations (ch50) recorded at the 1/3-

distance location of the main span of the deck. As done in Figure 4, the 5–95% normalized summed squared acceleration method yields the estimated structural strong shaking duration as ~60 seconds. When compared to ~13.25 seconds for the ground motion (Figure 4), there is a significant increase of 46.75s for the SAS. In Figure 10b, the additional "step-like" vibrational energy (as represented by the normalized summed squared acceleration) is added several times on a regular and repetitious basis, due to beating. The observed length of each beating cycle time (or beating period) differs for the vertical, as compared to transverse, acceleration time history. From this plot, the beating periods in the translational and vertical direction of the main span deck are extracted to be ~14.7 s and ~10.6 s, respectively. (c) As a result, the repetitious exchange between vibrational and potential energy that causes the elongated response may result in low-cycle fatigue of the elements of the suspension bridge (*e.g.*, the cables, hangers, deck, and tower). (d) Importantly, the data record length is important when computing summed squared acceleration time history because the record length of 149 s in the data set used in this study is based on a "start" and "end" recording acceleration threshold (as opposed to continuous recording and selecting the record length on demand). Thus, it is likely that the beating continues beyond the "stop recoding" threshold (149 s in this case), possibly elongating the shaking even more than the estimated ~60 s. (e) Finally, as stated earlier, important requisite conditions for beating effects to materialize are a low critical damping percentage of the structure and its components (tower, deck, and cables).

The N4SID system identification revealed critical damping percentages of <5% (varying between 2.11 and 4.83%). Critical damping percentage assessed by logarithmic decrement method is 1,43% as demonstrated in Figure 10c.

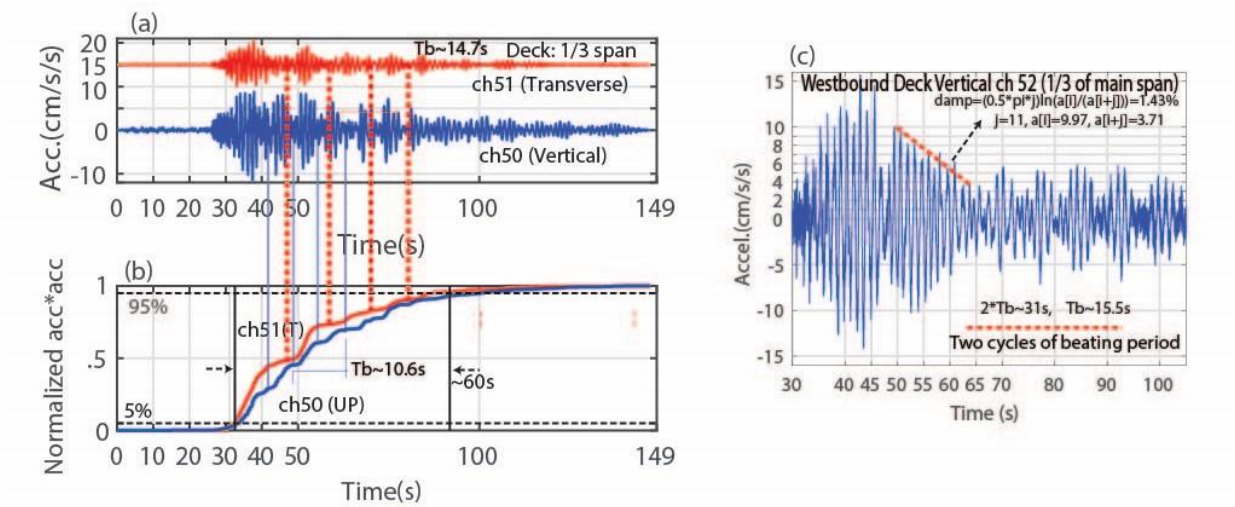

Figure 10. (a) Acceleration time histories of transverse channel 51 and vertical channel 50 (at the 1/3-distance span location of the main span deck), (b) normalized summed squared accelerations (step-like increases due to beating) and (c) A 30-105-second window of vertical acceleration time history of channel 52. The critical damping percentage (1.43%) is computed using logarithmic decrement method. Also displayed is the repetitious beating effect – (assessed beating period (T_b) is 15.5 s.

4.6. Apparent Frequency

The fact that frequencies and critical damping percentages are identified for the components (tower, deck, and cables) of the SAS does not allow for direct comparison with those characteristics, as computed for the total SAS structural system in its global coordinates (as has been done by Nader, Lopez-Jara, and Mibelli, 2002). Therefore, using the "apparent frequency" computation is appropriate to estimate global-coordinate-based frequencies for the SAS components (tower, deck, and cables). This is attempted even though the frequencies of the components are identified from low-amplitude shaking data. The Nader, Lopez-Jara, and Mibelli (2002) frequencies (periods) are computed for the much-larger-amplitude safety evaluation earthquake (SEE) event and for longitudinal, transverse, and vertical orientations of the SAS, respectively, as 0.263 Hz (3.80 s), 2.75 Hz (3.64 s) and 0.222 Hz (4.50 s).

The "apparent" frequency (f_a) approach is widely known and used in soil-structure analyses of buildings as: $1/f_a^2 = 1/f_1^2 + 1/f_2^2$, where f_1 and f_2 are the frequencies of the structure and soil, respectively (Jacobsen and Ayre, 1958; Luco, 1986, Trifunac et al., 2001). This relationship is described by Trifunac et al. (2001) as a

"combination rule", whereby f_a, (period, T_a) is shorter (longer) than the shortest frequencies (longest periods) of interacting parts. From the above relationship, the apparent frequency (f_a) and period (T_a) are computed directly as:

$$f_a = \sqrt{((f_1^2 . f_2^2)/ (f_1^2 + f_2^2))} \text{ or } T_a = \sqrt{(T_1^2 + T_2^2)}. \quad (2)$$

However, for the Golden Gate Bridge study (Çelebi, 2012), which also may be applicable for other long-span suspension bridges, when only the deck (f_{deck}) and tower (f_{tower}) are considered and when the difference between them is large enough, the apparent frequency is identical to the lower of the two - which always is that of the deck. For the Golden Gate Bridge, the apparent frequency (f_a) of 0.13 Hz was computed from the interacting tower's longitudinal (~ 0.7 Hz) and the deck's vertical (0.13 Hz) motions and is the same as the deck's vertical motion (0.13 Hz) (as computed by $f_a = \sqrt{((f_1^2 . f_2^2)/ (f_1^2 + f_2^2))}$).

Similarly, in the case of the Carquinez Suspension Bridge (Çelebi, Ghahari, and Taciroglu 2019), the tower longitudinal frequency (0.39 Hz) is significantly higher than that of the deck vertical frequency (0.17 Hz). The resulting apparent frequency, f_a (at ~ 0.17 Hz), is very close to f_{deck} (at 0.17 Hz).

Applying Equation 2 to the SAS and using the deck vertical frequency (period) as 0.25 Hz (4.0s) and the tower longitudinal frequency (period) as 0.3 Hz (3.33s), the apparent frequency (period), fa (Ta), is obtained as 0.19 Hz (5.20 s). Similarly, using the tower longitudinal frequency (period) as 0.3 Hz (3.33 s) and tower transverse frequency (period) as 0.33 Hz (3.0s), apparent frequency (period), fa (Ta), is obtained as 0.22 Hz (4.48 s). The apparent frequencies for these three bridges (the SAS, Golden Gate, and Carquinez bridges) are summarized in Table 1.

Table 1. Deck lengths, tower heights, and apparent fundamental periods for three suspension bridges.

Bridge	Deck Length (m/ft)		Tower Height Above (m/ft)		Deck (UP) Apparent T/f (s/Hz)
	Main Span	Total	Deck Level	Footing Level	
SAS (this study)	385/1263	622.5/2042	107/351	157/515	5.2/0.19
Golden Gate (Çelebi, 2012)	1280/4200	1996/6450	143/469	210/689	7.7/0.13
Carquinez (Çelebi, 2019)	728/2389	1056/3465	(T2) 78.47/257 (T3)79.46/261	(T2)116.72/382 (T3)122.76/403	5.9/0.17

Figure 11 displays the variation of apparent periods against both (a) the main span only and (b) the total length of the deck. There is surprisingly almost a linear variation, even though the SAS has only one tower and one side span. Naturally, more empirical data is required to make a claim of a reliable correlation.

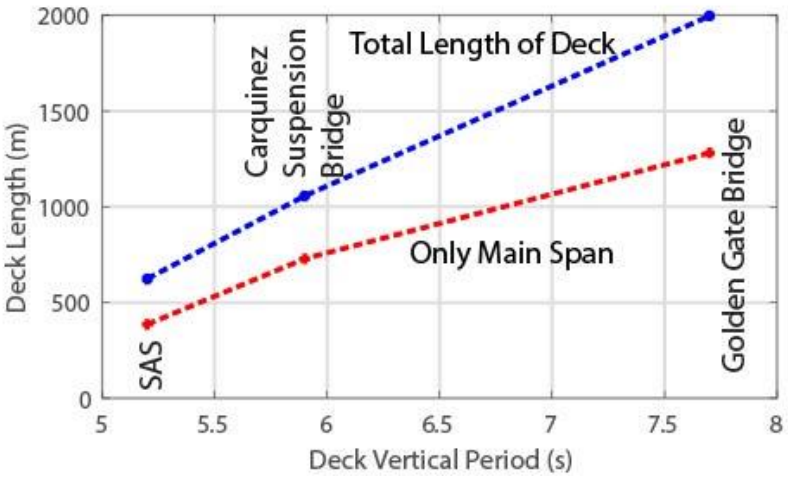

Figure 11. Comparison of earthquake-data-based apparent periods for the SAS (Self-Anchored Suspension), Golden Gate, and Carquinez Suspension bridges of the San Francisco Bay Area.

5. Summary, Discussions, and Conclusions

Data from seismic monitoring array of SAS recorded during low amplitude shaking caused by the October 14, 2019, M_w 4.6 Pleasant Hill earthquake are used in this study. “Global structural coordinates” (longitudinal, transverse, and vertical coordinates) defined for the overall SAS structure are also coordinates for the three main SAS components (tower, deck, and cables). Importantly, the sensors are deployed at select locations of the components. Hence, the identified structural dynamic characteristics (frequencies and critical damping percentages) from channel-based-data are affiliated with the particular components at which the sensors have been deployed, not the global SAS structure. The various spectral plots (many of which are for several sensors on the same component) presented in this paper indicate repeatable dominant modal frequencies as belonging to each component. Therefore, it is not possible to make a direct declaration of the dynamic characteristics for the overall SAS structure. All the identified fundamental frequencies (periods) and critical damping percentages of “components of the SAS” (tower, deck, and cables) in the “global coordinates” (longitudinal, transverse, and vertical directions) are summarized in Table 2.

From design era FEM analyses, only three fundamental periods (frequencies) [3.80 s (0.263 Hz), 3.64 s (0.275 Hz), and 4.50 s (0.222 Hz)] in the global (longitudinal, transverse, and vertical) coordinates for the overall SAS structure are publicly available (Nader, Lopez-Jara, and Mibelli (2002) for the much larger design input motions defined by the safety evaluation earthquake (SEE). For comparison, these fundamental frequencies (periods) are also included in Table 2. Of course, it is not valid to directly compare the dynamic response characteristics identified in this study (using low-amplitude shaking earthquake data) with those from the design-level SEE earthquake. Nonetheless, to make sense of the data-based identified data, a couple of “apparent” periods (frequencies) have been computed (and are included in Table 2) to be representative of the overall global structure. The computed apparent period for the vertical direction (5.20 s) is larger than the 4.50-second value obtained from the reported SEE analysis. The deduction, then, is that for a much larger strong shaking event, the apparent period will be even longer.

Table 2. Identified fundamental periods[s], (frequencies [Hz]), and damping of the deck, tower, and cables of the SAS and comparison with those computed during design phase analyses.

	Components of the SAS in Global Coordinates			
	L	T	UP	Damping (%)
	Spectral Ratios			
Deck	-	3.0/0.33	4.0/0.25	
Tower	3.33/0.30	3.0/0.33	-	
Cable	-		4.0/0.25	
	System Identification			
Deck		2.79/0.36	4.14/0.24	2.11% (T), 2.64%(UP)
Tower	2.14/0.47	2.79/0.36		3.14%(L) 4.83%(T)
Design/Analyses Assessment (Global Coordinates) Ref. Nader, Lopez-Jara and Mibelli (2002)				
T(s)/f(Hz)	3.80/0.263	3.64/0.275	4.50/0.222	
Logarithmic Decrement				1.43% (UP) Deck
Apparent Frequency [Hz]/(Period [s])				
			Deck(V)&Tower(L)	Tower (L) &Tower(T)
			5.20/0.19	4.48/0.22

Low critical damping percentages (~2-4.8% by N4SID system identification) and (1.43% by the logarithmic decrement) computations resulted in low critical damping percentages (~2-4.8%) and are all less than the usual 5% used in practice.

Closely coupled modes and low critical damping percentages led to responses with a significant beating effect, for which beating periods have been computed to be ~12-15 s. This behavior is observed in all acceleration and displacement time histories of the three structural components (tower, deck, and cables).

A linear trend between the fundamental vertical period of the deck and the deck length is observed for three suspension bridges. However, it is desirable to collect more data from SAS-type bridges (if others exist) and from conventional suspension bridges (with two-towers and anchorages at two ends of the deck) to develop a more robust and reliable correlation.

Any use of trade, firm, or product names is for descriptive purposes only and does not imply endorsement by the U.S. Government.

6. References

Boore D. M. and Thompson E. M. 2014. Path Durations for Use in the Stochastic-Method Simulation of Ground Motions, *Bulletin of the Seismological Society of America*, Vol. 104, No. 5, pp. 2541–2552, October 2014, doi: 10.1785/0120140058.

Boroschek R.L. and Mahin S. A. 1991. Investigation of the seismic response of a lightly-damped torsionally-coupled building. Earthquake Engineering Research Center Report UCB/EERC-91/18, University of California, Berkeley. 291 pp.

Çelebi M. 2012. Golden Gate Bridge Response: A Study with Low-Amplitude Data from Three Earthquakes. *Earthquake Spectra*. 28. 2, pages 487–510.

Çelebi M. 2018. Quantifying the effect of beating inferred from recorded responses of tall buildings. Proceedings of the 11th National Conference in Earthquake Engineering, Earthquake Engineering Research Institute, Los Angeles, CA. June 25–29, 2018.

Çelebi M., 2019, Ghahari S.F. and Taciroglu E., Responses of the odd couple Carquinez, CA, suspension bridge during the Mw6.0 South Napa earthquake of August 24, 2014, 2019*, Journal of Civil Structural Health Monitoring*. 9 .5. pp. 719-739, DOI 10.1007/s13349-019-00363-6

Çelebi M., Haddadi H.. Huang M., Valley M., Hooper J. and Klemencic R., 2019, The Behavior of the Salesforce Tower, the Tallest Building in San Francisco, California Inferred from Earthquake and Ambient Shaking, *Earthquake Spectra.* 35. 4. pp 1711–1737. (https://doi.org/10.1193/112918EQS273M).

Çelebi M., 2023, The new self-anchored suspensión bridge of the San Francisco Bay Bridge System: A preliminary study of the response and behavior during a small earthquake.

Frick K. T. 2016. Remaking the San Francisco–Oakland Bay Bridge: A Case of Shadowboxing with Nature. First published 2016, Routledge Publishing, 711 Third Avenue, New York, NY 10017, 185 pages.

Jacobsen L. S., and Ayre R. S., 1958, Engineering Vibrations, McGraw-Hill, New York, 564 pp.

Kim S., Pakzad S., Culler D., Demmel J., Fenves G., Glaser S., and Turon M. 2007. Health monitoring of civil infrastructures using wireless sensor networks. Proceedings of the Int'l Conf. on Information Processing in Sensor Networks (IPSN '07), Cambridge, MA., ACM Press, 254–264.

Ljung L. 1987. *System Identification: Theory and User*. Prentice Hall, Upper Saddle River, NJ, 672 pp.

Luco J. E., Wong H. L., and Trifunac M. D.1986, Soil-Structure Interaction Effects on Forced Vibration Tests, Department of Civil Engineering Report No 86-05, University of Southern California, Los Angeles, CA.

Mathworks. 2020, Matlab Users Guide. System Identification Toolbox for use with Matlab. The Mathworks Inc.: South Natick, MA.

McDaniel C. C., Uang C-M., and Seible F. 2003. Cyclic Testing of Built-Up Steel Shear Links for the Bay Bridge. ASCE *Journal of Structural Engineering*. 129. 6, June 1, 2003.

Nader M., Lopez-Jara J. and Mibelli C. 2002, Seismic design strategy of the new San Francisco-Oakland Bay Bridge Self Anchored Suspension Span. *in* Proceedings of the Third National Seismic Conference on Bridges and Highways: April 28-May 1, 2002, p. 109.

Nader M., Duxbury J., and Maroney B. 2014. Seismic Design of the Self Anchored Suspension San Francisco Oakland Bay Bridge, 37th International Association for Bridge and Structural Engineering (IABSE) Symposium. Madrid. September 2014 Report. vol. 102, no. 21, pages 1307-1314.

Penzien J. (Chairman), Seible F., Bolt B. A., Idriss J.M., Nicoletti R.F., Preece J., Roberts J.E., (ed. Chuck Thiel), 2003. Board, Caltrans Seismic Advisory. "The Race to Seismic Safety." *Report to the Director of*

California Department of Transportation on Protecting California's Transportation System, 186 pages.

Sun J., Manzanarez R., and Nader M. 2004. Suspension Cable Design of the New San Francisco–Oakland Bay Bridge. ASCE, *Journal of Bridge Engineering.* 9. 1. pp.101–106.

Trifunac M. D. and Brady A. G. 1975. A study on the duration of strong earthquake ground motion. *Bulletin of the Seismological Society of America.* 65. 3. pp. 581-626.

Trifunac M. D., Ivanovic S. S., and Todorovska M. I. 2001. Apparent periods of a building: Fourier analyses, ASCE *Journal of Structural Division*, 127, 517–526.

Van Overschee P., and De Moor B., 1996, Subspace Identification for Linear Systems. Dordrecht: Kluwer Academic Publishers.